Feature Extraction of Conductor Galloping for Transmission Lines: A Non-Contact Method Using Magnetic Field Sensing

Yalong Mai[1], Jian Li[1,*], *Senior Member, IEEE*, Yankai Xing[1], Haopeng An[1], and Guangdou Zhang[2]
1. The Low Carbon Intelligent Power and Energy System Key Laboratory of Sichuan Province,
University of Electronic Science and Technology of China, China
ylmai@std.uestc.edu.cn, {leejian, xingyankai}@uestc.edu.cn, haopengan@std.uestc.edu.cn
2. Department of Electrical Engineering, Tsinghua University, China
gdzhang@mail.tsinghua.edu.cn

***Abstract*—Conductor galloping feature extraction is widely recognized as a core foundation for understanding galloping mechanisms and mitigating galloping-induced disasters. However, traditional methods are confronted with inherent challenges in practical engineering scenarios, including limited adaptability to extreme environments and prohibitive deployment costs. To address these limitations, a low-cost, deployable, and high-reliability non-contact galloping feature extraction method based on magnetic sensing is proposed, which utilizes spatial magnetic fields at two points above the conductor to reconstruct the conductor galloping trajectory and extract galloping frequency and amplitude. The effectiveness of the proposed method is validated through experiments conducted on a scaled-down laboratory model. The method demonstrates significant engineering application potential in galloping feature extraction under extreme operating conditions and operational risk assessment.**

***Index Terms*—conductor galloping, feature extraction, magnetic sensing.**

I. INTRODUCTION

Transmission lines serve as primary channels for energy transmission, and their safe and reliable operation is of paramount importance to the stability of power systems and the security of energy supply. However, these lines are frequently exposed to extreme climatic conditions, particularly in high-altitude and low-temperature regions, where conductors with uneven icing are prone to generating low-frequency and large-amplitude galloping under wind excitation. Conductor galloping (CG), characterized by long duration and wide impact range, stands as a primary risk factor threatening the mechanical safety of transmission lines, and is prone to causing severe consequences such as fatigue damage of fittings, wear of insulators, and instability of towers [1].

In recent years, the academic community has conducted extensive research on galloping mechanisms and prevention strategies [2], [3], among which the extraction of galloping characteristic parameters (i.e., the identification and quantification of key parameters such as galloping frequency, amplitude, and motion trajectory) serves as the core foundation for in-depth understanding of galloping mechanisms and effective implementation of galloping disaster prevention. Furthermore, through the extraction of galloping characteristic parameters and the construction of a feature database, critical support is provided for the realization of intelligent identification and accurate prediction of CG using artificial intelligence methods.

Conventional conductor galloping monitoring techniques mainly include the acceleration sensing method [4], fiber optic sensing method [5], [6], and image recognition method [7], [8]. The contact-based acceleration method retrieves galloping parameters via acceleration signals inversion but requires power outages for installation, incurs high costs, and faces strict insulation demands in high-voltage scenarios. Fiber optic sensing uses bonded fiber Bragg gratings (FBGs) to detect conductor strain or optical signal variations but suffers from microbending loss caused by thermal expansion/contraction and icing with high laying costs in complex terrain. Image recognition identifies galloping features through camera data and algorithmic extraction but is severely limited by lighting conditions (e.g., reduced accuracy at night or in fog) and lacks reliability in extreme weather. In summary, existing approaches cannot reliably extract line galloping characteristics in extreme environments, necessitating a novel low-cost, non-contact, highly reliable, and environmentally adaptive technology.

To overcome the limitations of existing technologies in extracting galloping characteristics under complex environmental conditions, a non-contact galloping characteristic extraction method based on magnetic sensing is proposed in this paper, leveraging the inherent property that magnetic fields are not interfered with by environmental and climatic factors. The primary contributions of this paper are summarized as follows:

(1) A spatial MF distribution model during CG is established, and a set of characteristic parameters for describing CG via magnetic fields is proposed.

(2) A method for reconstructing the galloping trajectory of the conductor and extracting galloping frequency and amplitude by utilizing spatial MF at two points above the conductor is proposed, the feasibility of which is verified in experiments.

979-8-3315-8138-1

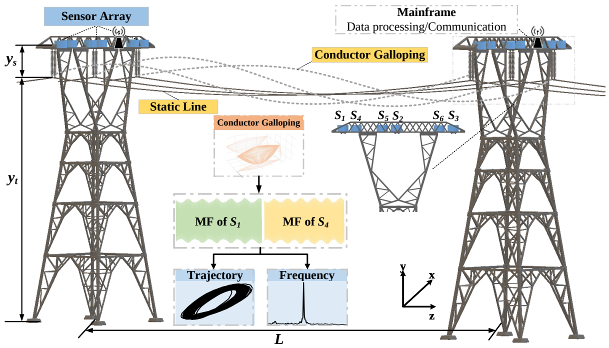

Fig. 1. Overall Architecture Diagram of the Conductor Galloping Feature Measurement System for a Typical Three-Phase Transmission Line. Sensors are placed at the crossarm above the conductor, and two adjacent sensors measure the galloping parameters of a single conductor.

II. Magnetic Field Distribution Model Under Conductor Galloping

A. Motion Equation of CG

Conductor galloping is a low-frequency, large-amplitude self-excited oscillation induced by icing and wind excitation. Existing studies generally consider conductor galloping as a vibration with 3 degrees of freedom, namely in-plane, out-of-plane, and torsional directions. However, under normal circumstances, the lateral galloping of conductors is more likely to cause damage to the line. Therefore, for the purpose of simplifying the analysis, a simplified two-degree-of-freedom model (considering in-plane and out-of-plane galloping) is widely adopted by many scholars. Taking the ground below the middle-phase conductor as the coordinate origin, the direction of conductor extension as the z-axis, the direction perpendicular to the conductor as the x-axis, and the vertical direction as the y-axis to establish a coordinate system, the equation of motion for CG can be described by the following standing wave equation:

$$\begin{cases} y_p = A_i sin(2\pi f_i t + \varphi_i) sin(\frac{n_i \pi z_p}{L}) + y_{st}, \\ x_p = A_o sin(2\pi f_o t + \varphi_o) sin(\frac{n_o \pi z_p}{L}) + l_p, \end{cases} \quad (1)$$

where y_{st} is represented as:

$$y_{st} = s(\frac{2z_p - L}{L})^2 + y_t - s \quad (2)$$

Here, $A_{i,o}$ denotes the gallop amplitude in the vertical and horizontal directions, $f_{i,o}$ represents the oscillation frequency, and $\varphi_{i,o}$ refers to the initiation phase, $n_{v,h}$ denotes the galloping order. Additionally, l_p represents the horizontal coordinate of each conductor in the stationary state, s is the sag value in the stationary state, L stands for the span, and y_t represents the tower height.

B. MF Distribution Under CG

Previous studies [9] have indicated that, when the sensor is positioned at the location illustrated in the Fig.1, the MF in the x-axis direction not only accounts for the largest proportion but also exhibits the highest sensitivity to variations in the spatial position of the conductor. Therefore, only the MF in the x-axis direction is considered in this paper. According to the Biot-Savart law, the spatial MF in the x-axis (B_{Xps}) generated by the current at a certain point in space (x_s, y_s, z_s) is expressed as:

$$B_{X_{ps}} = \hat{i}_x \frac{\mu_0 I_p}{4\pi} \int_{-L}^{L} \frac{\frac{\partial y_p}{\partial z_p}(z_s - z_p) - (y_s - y_p)}{|(x_s - x_p) + (y_s - y_p) + (z_s - z_p)|^3} \mathrm{d}z_p \quad (3)$$

Here, μ_0 is permeability of vacuum, I_p denotes phase current of a single wire. The product of the remaining parts in Equation (3) excluding the current I_p is denoted as $A_{X_{ps}}$, which exhibits a complex integral form and has no explicit expression. This paper simplifies it into the following expression by means of curve fitting:

$$A_{Xps}(t) = \begin{cases} A^0_{Xps} + k^i_p A^i_p \sin\theta^i_p, & \text{if } s = p, \\ A^0_{Xps} + k'^i_p A^i_p \sin\theta^i_p + k^o_p A^o_p \sin\theta^o_p, & \text{if } s = p + 3, \\ A^0_{Xps}, & \text{otherwise,} \end{cases} \quad (4)$$

where

$$\theta^i_p = 2\pi f^i_p t + \varphi^i_p, \theta^o_p = 2\pi f^o_p t + \varphi^o_p. \quad (5)$$

Here, A^0_{Xps} represents the MF contribution coefficient of the conductor in its static state, k^i_p, k'^i_p and k^o_p are the linearity coefficient, denoting the linearity relationship between the galloping amplitude $A^{i,o}_p$ and A_{Xps}, and θ^i_p, θ^o_p is related to the galloping frequency. The MF generated by multi-phase conductors are coupled in space and are expressed as linear superposition. Therefore, for a three-phase conductor system, the MF at a point in the surrounding space can be expressed as:

$$B_{X_s}(t) = \sum_{p=1}^{3} A_{X_{ps}}(t) I_p(t). \quad (6)$$

III. Feature Extraction of CG Based on Magnetic Field Sensing

A. Construction of Galloping Feature Parameters

The MF at sensors S_1 and S_4 near phase A are analyzed as examples, and the analysis methods for the remaining sensors are consistent with this. According to (4) and (6), when the A-conductor gallops, the MF of S_1 and S_4 are expressed as:

$$B_{X1}(t) = (A_{X11}(t)I_1(t) + A^0_{X21}(t)I_2(t) + A^0_{X31}I_3(t)), \quad (7)$$

$$B_{X4}(t) = (A_{X14}(t)I_1(t) + A^0_{X24}(t)I_2(t) + A^0_{X34}I_3(t)). \quad (8)$$

Take the moment of maximum phase A current as the observation moment, and according to previous research conclusions [10] (i.e., the moment of maximum current is approximately equivalent to the moment of maximum MF), Equations (7)-(8) are rewritten as:

$$B_{X_{1RMS}}(t) = (A_{X11}(t) + \beta A^0_{X21} + \gamma A^0_{X31}) I_{1RMS}, \quad (9)$$

$$B_{X_{4RMS}}(t) = (A_{X14}(t) + \beta A_{X24}{}^0 + \gamma A^0_{X34}) I_{1RMS}, \quad (10)$$

where $B_{X_{pRMS}}$ denotes the effective value of MF, I_{1RMS} denotes the effective value of current, and β and γ denote

979-8-3315-8138-1

respectively the ratios of phase A current to B and C currents at this moment. Substituting (4) into (9) and (10) and simplifying, we can obtain:

$$B_{X_{1RMS}}(t) = B^0_{X_{1RMS}} + k_1^i A_1^i \sin\theta_1^i I_{1RMS} \quad (11)$$

$$B_{X_{4RMS}}(t) = B^0_{X_{4RMS}} + (k_1'^i A_1^i \sin\theta_1^i + k_1^o A_1^o \sin\theta_p^o) I_{1RMS} \quad (12)$$

where

$$B^0_{X_{1RMS}} = (A^0_{X11} + \beta A^0_{X21} + \gamma A^0_{X31}) I_{1RMS} \quad (13)$$

$$B^0_{X_{1RMS}} = (A^0_{X14} + \beta A^0_{X24} + \gamma A^0_{X34}) I_{1RMS} \quad (14)$$

Further simplifying (11) and (12), the characteristic quantities T_x and T_y directly related to CG can be extracted:

$$T_y(t) = k_1^i A_1^i \sin\theta_1^i \quad (15)$$

$$T_x(t) = k_1'^i A_1^i \sin\theta_1^i + k_1^o A_1^o \sin\theta_1^o \quad (16)$$

where,

$$T_y(t) = (B_{X_{1RMS}}(t) - B^0_{X_{1RMS}})/I_{1RMS} \quad (17)$$

$$T_x(t) = (B_{X_{4RMS}}(t) - B^0_{X_{4RMS}})/I_{1RMS} \quad (18)$$

Here T_x and T_y denote the ratio of the effective value of MF at the sensor (after filtering out the DC component) to the effective value of current. The effective value of current can be obtained via the current transformer at the line terminal. The constructed characteristic parameter T_x and T_y can clearly and directly reflect the amplitude and frequency characteristics of CG.

B. CG Trajectory Reconstruction Based on MF Sensing

In most cases, the in-plane and out-of-plane galloping frequencies of the conductor are consistent, with an initial oscillation phase difference $\Delta\varphi$ between them, and its cross-sectional motion trajectory takes the shape of the most common oblique ellipse. In this case, rewrite (16) as:

$$\begin{aligned} T_x(t) &= k_1'^i A_1^i \sin\theta_1^i + k_1^o A_1^o \sin(\theta_1^i + \Delta\varphi) \\ &= (k_1'^i A_1^i + k_1^o A_1^o \cos\Delta\varphi)\sin\theta_1^i + k_1^o A_1^o \sin\Delta\varphi \cos\theta_1^i \end{aligned} \quad (19)$$

To simplify the expression and the equations, we define the following variables:

$$C_1 = k_1'^i A_1^i + k_1^o A_1^o \cos\Delta\varphi \quad (20)$$

$$C_2 = k_1^o A_1^o \sin\Delta\varphi \quad (21)$$

$$K = k_1^i A_1^i \quad (22)$$

By combining (15), (19), (20)-(22) and simplifying, we eventually derive the trajectory equation of the galloping characteristic parameters T_x and T_y defined in this paper:

$$K^2 T_x^2 - 2KC_1 T_x T_y + (C_1^2 + C_2^2) T_y^2 = K^2 C_2^2 \quad (23)$$

This is a typical elliptic equation. Based on the above conclusion, it is found that during CG, the characteristic parameters T_x and T_y constructed using the MF at two points on the tower are capable of mapping the CG trajectory, and meanwhile, using these characteristic parameters, the frequency, amplitude, and trajectory of CG can be effectively reconstructed. Actually, the core characteristic of multimodal galloping is internal resonance: the frequencies of in-plane and out-of-plane galloping typically exhibit integer ratios such as 1:1 and 1:2. According to the definition in (15)-(16), the superposition of simple harmonic vibrations T_y and T_x forms a Lissajous figure, where the trajectory degenerates into an oblique ellipse when the frequency ratio is 1:1 and takes the shape of '∞' when the ratio is 1:2.

C. Measurement of CG Frequency and Amplitude

According to (15)-(16), the galloping characteristic parameters T_x and T_y contain the CG frequency. By performing Fast Fourier Transform (FFT) on them to extract the main frequency, the CG frequency can be obtained. For the galloping amplitude of the conductor, it can be solved by substituting special values into the equation. According to Equation (15), the in-plane galloping amplitude can be obtained by substituting the maximum and minimum values of T_y:

$$A_1^i = (T_{y_{max}} - T_{y_{min}})/2k_1^i \quad (24)$$

According to (15) and (16), when $T_y = 0$, $\theta_1^i = 0$ or π, and at this time T_x is:

$$X_1 = k_1^o A_1^o \sin\Delta\varphi, X_2 = k_1^o A_1^o \sin(\pi f_1^o/f_1^i + \Delta\varphi), \quad (25)$$

where

$$\Delta\varphi = \varphi_1^o - \varphi_1^i f_1^o/f_1^i \quad (26)$$

When $T_y = T_{y_{max}}$, $\theta_1^i = \frac{\pi}{2}$, and at this time T_x is:

$$X_3 = k_1'^i A_1^i + k_1^o A_1^o \cos\Delta\varphi \quad (27)$$

By combining (25)-(27), the out-of-plane galloping amplitude can be obtained:

$$A_1^o = \sqrt{X_1^2 + (X_3 - k_1'^i A_1^i)^2}/k_1^o, f_1^o = f_1^i \quad (28)$$

$$A_1^o = \sqrt{X_1^2 + \left(\frac{X_2 - X_1\cos\left(\pi f_1^o/f_1^i\right)}{\sin\left(\pi f_1^o/f_1^i\right)}\right)^2}/k_1^o, f_1^o \neq f_1^i \quad (29)$$

It can be seen from (28)-(29) that when the in-plane and out-of-plane galloping frequencies are consistent, (28) is used to calculate the out-of-plane galloping amplitude, while when the frequencies are inconsistent, (29) is used for the amplitude calculation.

D. Algorithm of The Proposed Method

Based on the above method, a galloping feature extraction algorithm was developed as shown in Fig. 2. First, within the sampling time window w_d, extract the effective value of MF for each cycle of the sensor. In accordance with Eqs. (17) and (18), calculate the galloping feature parameters T_x and T_y. Connecting each point ($T_x[N]$, $T_y[N]$) in the sequence

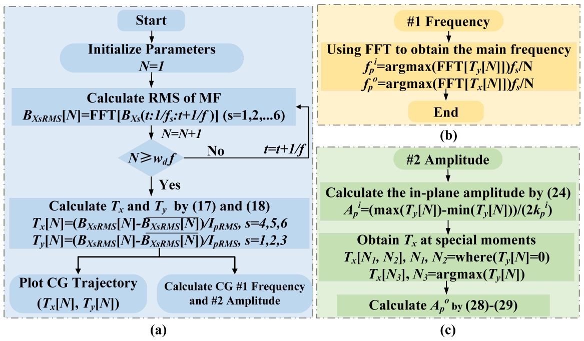

Fig. 2. Flowchart of the Proposed Galloping Feature Extraction Algorithm.

TABLE I
PARAMETER SETTINGS OF SCALED MODELS FOR EXPERIMENTS

Parameter	Value	Parameter	Value
Span (L)	5 m	Inter-phase Space (l_p)	0.5 m
Tower height (y_t)	1.59 m	k_1^i	9.97
Sag (s)	0.32 m	$k_1'^i$	4.38
Phase Current (I_p)	15.2 A	k_1^o	5.80

yields the trajectory diagram of CG. For galloping frequency extraction, perform FFT on T_x and T_y and find the index with the maximum amplitude in the sequence. For amplitude extraction, first calculate the in-plane galloping amplitude using (24), and then substitute the special points ($T_x[N_1]$, 0), ($T_x[N_2]$, 0) and ($T_x[N_3]$, T_{ymax}) into (28)-(29) to obtain the out-of-plane galloping amplitude.

IV. EXPERIMENTAL VALIDATION

A. Experimental Setup

To verify the effectiveness of the proposed method, experimental verification was conducted on a scaled-down model built in the laboratory with a scaling factor of 20:1, where the tower uses the same steel material as the actual tower. A three-phase voltage regulator is used to adjust the conductor current, and a digital clamp meter is used to measure the conductor current. The load consists of 6 resistors with a resistance of 5 ohms and a capacity of 4 kW. A DC power supply provides power for the mainframe and the magnetic field sensor, and the mainframe is responsible for clock synchronization and sending data to the desktop via the serial port.

Sensing units are placed on the upper part of the tower after calibration. Based on simulation results, the MF range at the sensor position in actual scenarios spans from several microteslas to a maximum of several hundred microteslas. Within this range, the TMR2103 exhibits excellent linearity and boasts high resolution (0.01 μT), enabling it to effectively capture MF variations induced by galloping. The data processing circuit includes an instrumentation amplifier (used for filtering out common-mode interference), a band-pass filter (used for improving the signal-to-noise ratio (SNR) of the signal), a programmable amplifier (used for signal amplification), and a microprocessor (used for analog-to-digital conversion).

B. Key Feature Extraction of Galloping

To verify the effectiveness of the proposed galloping feature extraction method based on MF measurement, this paper

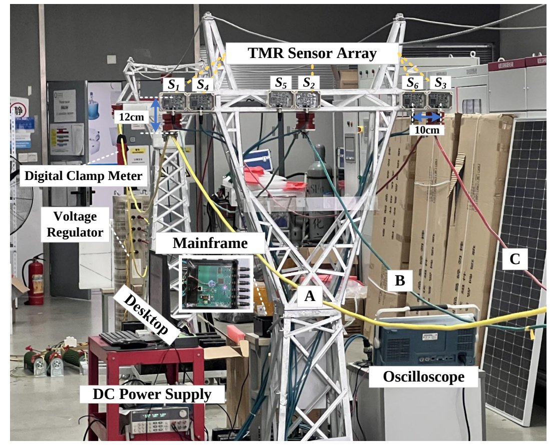

Fig. 3. Construction of scaled overhead transmission lines in laboratory environment.

conducted three simulated galloping experiments on the Phase A conductor in a scaled model, where Case 1 and Case 2 correspond to 1:1 ratio galloping, while Case 3 represents 1:2 internal resonance galloping. Fig.4 presents the experimental results of Case1 and Case3, where (a) and (e) show the time-varying curves of MF strength for S_1 and S_4 under different galloping conditions. It is evident that the MF exhibits distinct sinusoidal fluctuation characteristics during galloping. According to (17)-(18), the galloping characteristic parameters T_y and T_x under these two conditions are extracted, as shown in (b) and (f) respectively. It can be observed that the parameter T_x related to out-of-plane galloping exhibits significant frequency differences under different galloping modes. Through frequency feature extraction of galloping characteristic parameters using FFT, it can be seen that there is only one vibration frequency in Case 1, which is the natural frequency of the conductor at 1.7 Hz, while Case 3 (as shown in Fig. 4 (g) and (h)) has two frequencies with a ratio of 1:2 (1.7 Hz and 0.85 Hz). The CG frequency, amplitude, and phase difference between in-plane and out-of-plane galloping measured by the proposed method are shown in Table II, and the reconstructed CG trajectory is shown in Fig. 5. As can be seen from Fig. 5, for Case1 and Case2, the in-plane and out-of-plane galloping frequencies are identical with only a phase difference existing between them, forming an oblique elliptical trajectory. And the larger the phase difference, the closer the major axis of the ellipse is to the y-axis. In contrast, due to the 1:2 vibration frequency ratio, the motion trajectory of Case3 approximates a '∞' shape. The experimental results verify the effectiveness of using spatial MF in reconstructing the conductor galloping trajectory and extracting key galloping features.

C. Uncertainty Anysis in Real-world Scenarios

Measurement uncertainty of the proposed method in practical engineering applications must be considered. Through simulation validations, MF interference from adjacent phase conductors can be regarded as a constant MF offset (as

979-8-3315-8138-1

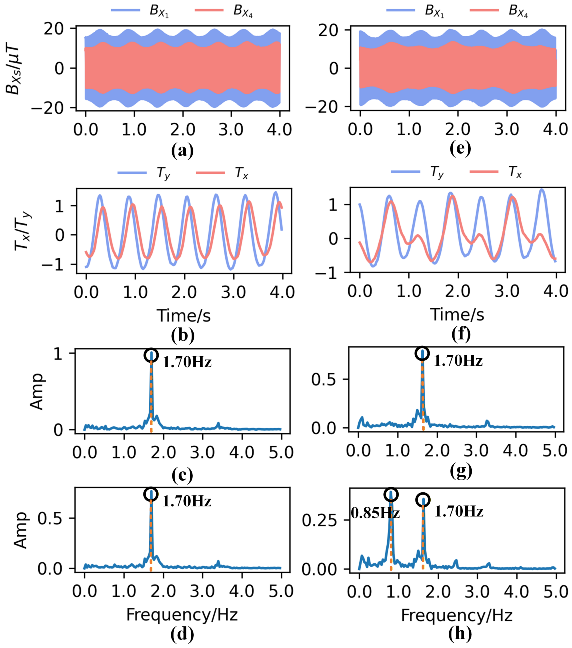

Fig. 4. Measurement Result Diagram of Conductor Galloping in Case1 and Case3. (a), (e) Time-varying Curve of MF at Sensors S_1 and S_4 during Galloping. (b), (f) Variation of Proposed Galloping Feature Parameters. (c), (d) Frequency Distribution Diagram of T_y and T_x in Case1. (g), (h) Frequency Distribution Diagram of T_y and T_x in Case3.

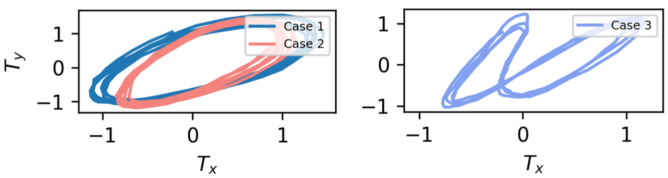

Fig. 5. Trajectory Diagram of Conductor Galloping in experiments.

shown in (11)-(14)), which has no impact on the proposed method. MF attenuation caused by towers is less than 1% [10], and can be mitigated by field calibration. Low-frequency MF from geomagnetic activities and high-frequency MF from radio sources have been filtered out by hardware-integrated band-pass filters. The MF measurement error caused by the power frequency component in industrial noise is typically less than 1% and can be eliminated through field calibration. Simulation results show that when the SNR reaches 60 dB or higher, measurement accuracy is within 5%. In low SNR scenarios, measurement errors can be reduced by averaging multiple measurements. Furthermore, simulation validations indicate that current imbalance, phase offset, and current harmonics have minimal impact on the measurement method, demonstrating its applicability in complex operating conditions. Sensor installation deviations affect measurement accuracy through k_p^i, $k_p^{\prime i}$ and k_p^o. Calculations reveal that a 5% positional deviation along the y-axis introduces approximately 5% measurement error for in-plane galloping amplitude, while a 5% deviation along the x-axis causes around 10% error for out-of-plane galloping amplitude. Installation position-induced measurement errors can be eliminated by calibrating k_p^i, $k_p^{\prime i}$ and k_p^o with precise positions obtained via laser rangefinders or similar tools.

TABLE II
MEASUREMENT RESULTS OF FREQUENCY, AMPLITUDE, AND PHASE DIFFERENCE OF CONDUCTOR GALLOPING

	In-plane		**Out-of-plane**		
Case	Frequency	Amplitude	Frequency	Amplitude	$\Delta\varphi$
Case 1	1.70 Hz	0.132 m	1.70 Hz	0.167 m	64.21°
Case 2	1.70 Hz	0.136 m	1.70 Hz	0.096 m	75.72°
Case 3	1.70 Hz	0.121 m	0.85 Hz	0.110 m	83.32°

V. CONCLUSION

In this paper, a novel non-contact method based on MF sensing for extracting galloping features is proposed. The method constructs galloping feature parameters by utilizing the MF intensity at two spatial points above the conductor, thereby enabling the measurement of CG frequency, amplitude, and motion trajectory. Experimental verification was conducted using a scaled model to validate the feasibility of the proposed method. Meanwhile, the uncertainty of the method's application in real-world scenarios has been fully taken into account. The proposed method holds significant engineering application potential for operational risk assessment in scenarios involving extreme operating conditions. This is our preliminary investigation into the application of MF sensing technology in galloping monitoring. In future research, we will conduct in-depth studies on its application in different tower structures, optimization of measurement point locations, and adaptability to low SNR scenarios.

REFERENCES

[1] Z. Mou, B. Yan, X. Lin, G. Huang, and X. Lv, "Prediction method for galloping features of transmission lines based on fem and machine learning," *Cold Regions Science and Technology*, vol. 173, p. 103031, 2020.

[2] F. Cui, X. Liu, S. Zhang, A. Zhou, and B. Huo, "The impact of interphase spacers on galloping control of three-phase iced eight-bundled transmission lines: An experimental study," *IEEE Transactions on Power Delivery*, vol. 36, no. 1, pp. 371–382, 2020.

[3] A. Zhou, X. Liu, S. Zhang, F. Cui, and P. Liu, "Wind tunnel test of the influence of an interphase spacer on the galloping control of iced eight-bundled conductors," *Cold Regions Science and Technology*, vol. 155, pp. 354–366, 2018.

[4] F. Zanelli, M. Mauri, F. Castelli-Dezza, D. Tarsitano, A. Manenti, and G. Diana, "Analysis of wind-induced vibrations on hvtl conductors using wireless sensors," *Sensors*, vol. 22, no. 21, p. 8165, 2022.

[5] T. Tan, C. Duan, X. Liu, D. Fan, Z. Ye, K. Xie, Q. Chai, Y. Tian, and J. Zhang, "Research on monitoring the transmission line tension and galloping based on fbg fitting sensor," *IEEE Transactions on Instrumentation and Measurement*, vol. 71, pp. 1–8, 2022.

[6] Q. Yan, C. Zhou, X. Feng, C. Deng, W. Hu, and Y. Xu, "Galloping vibration monitoring of overhead transmission lines by chirped fbg array," *Photonic Sensors*, vol. 12, no. 3, p. 220310, 2022.

[7] X. Huang, L. Yang, Y. Zhang, Y. Zhu, and G. Zhang, "A measurement technology of space distance among transmission bundle conductors based on image sensors," *IEEE Transactions on Instrumentation and Measurement*, vol. 68, no. 10, pp. 4003–4014, 2018.

[8] Y. Gao, J. Yang, K. Zhang, H. Peng, Y. Wang, N. Xia, and G. Yao, "A new method of conductor galloping monitoring using the target detection of infrared source," *Electronics*, vol. 11, no. 8, p. 1207, 2022.

[9] A. H. Khawaja and Q. Huang, "Estimating sag and wind-induced motion of overhead power lines with current and magnetic-flux density measurements," *IEEE Transactions on Instrumentation and Measurement*, vol. 66, no. 5, pp. 897–909, 2017.

[10] Y. Mai, Y. Xing, G. Zhang, H. Fan, J. Li, A. H. Khawaja, and Q. Huang, "A magnetic measurement-based contactless method for current/sag monitoring in overhead lines considering practical engineering conditions," *Measurement*, p. 118779, 2025.

979-8-3315-8138-1